Turkish Journal of Electrical Engineering & Computer Sciences

http://journals.tubitak.gov.tr/elektrik/

Research Article

Turk J Elec Eng & Comp Sci
(2016) 24: 1838 – 1846

doi:10.3906/elk-1311-159

Computation of the scattered fields from an arbitrary discontinuity on a perfectly conducting ground plane by a decomposition method

Uğur SAYNAK[1,*], **Ahmet KIZILAY**[2]

[1]TÜBİTAK Informatics and Information Security Research Center (BİLGEM), Gebze, Kocaeli, Turkey

[2]Department of Electronics and Communications Engineering, Faculty of Engineering, Yıldız Technical University, Esenler, İstanbul, Turkey

Received: 19.11.2013 • **Accepted/Published Online:** 01.07.2014 • **Final Version:** 23.03.2016

Abstract: A novel procedure for solving plane wave incident on arbitrary bump or cavity geometries on a perfectly conducting ground plane is introduced. The method is presented with examples for transverse-magnetic polarization compared to various other solution methods. The proposed method can be easily generalized to other similar problems.

Key words: Perturbation methods, method of moments, computational electromagnetics, rough surfaces

1. Introduction

Discontinuity problems on a ground plane can be considered as a popular research topic and can be applied to many real life problems like ground penetrating radar applications, propagation modeling over the earth, etc. These problems have been studied by many authors; solution methods include eigenfunction and analytical solutions for canonical discontinuities [1–9], method of moments (MoM) solutions [10–12], and various other methods [13–18]. A decomposition method involving perturbated fields excited by perturbated current densities [19–21] is calculated by MoM. The method includes an uncomplicated formulation and it can be simply generalized to other problems. It is applied to the problem of targets above [19,20] and below [21] sinusoidal surfaces. However, the application of this method to the bump or indent problem is not trivial. For the bump or indent case, the considered target has an intersection between two regions. The method assumes that impact of the discontinuity on the ground plane current density is rapidly fading away from the discontinuity and can be taken into account by frequency domain integral equations involving free space Green's functions like other objects in the calculation domain. Throughout this paper, the $e^{-j\omega t}$ time-harmonic factor is assumed and suppressed.

In the case of a bump on a perfectly conducting half space, half space Green's functions can be used to obtain a solution with MoM [22]. For an indent problem, dual integral equation solutions are required in order to overcome the nonuniqueness of the solution in the case of cavity resonances [23], which have considerably complex formulations compared to the bump problem.

In the next section, problems will be described with the proposed solution method for transverse-magnetic (TM) polarization. In the following section, solutions will be verified by comparison with the various reference results for circular and triangular bump geometries on a perfectly conducting plane. Afterwards, circular, elliptical, rectangular, and triangular cavity geometries in a ground plane will be investigated.

*Correspondence: ugur.saynak@tubitak.gov.tr

2. Statement of the problem

Scattering problems are two-dimensional arbitrary discontinuities on an infinite perfectly conducting ground plane, as depicted on Figure 1.

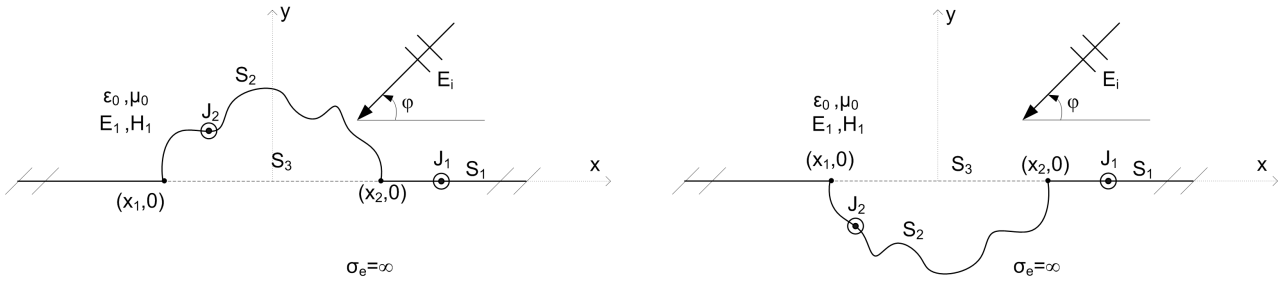

Figure 1. Scattering geometries: (a) bump, (b) indent.

Here S_2 is the bump or cavity cross-section surface, S_3 is the surface that will be absent when the discontinuity is present, and S_1 is the infinite perfectly conducting plane lying on the x axis. A TM polarized plane wave

$$\vec{E}^i = e^{jk\left(x\cos\varphi^i + y\sin\varphi^i\right)}\hat{z} \tag{1}$$

is incident on discontinuity with arbitrary cross-section with the incidence angle φ^i. Here, k is the free space wavenumber. The source of the incident plane wave field is sufficiently far away from the scatterers such that no additional image charges exist. The scattered field due to this incident field must satisfy the radiation condition. The discontinuity surface is regular such that the fields and their derivatives are continuous on the boundaries. If the discontinuity is absent, the calculation domain is free space for $y > 0$ and perfectly conducting for $y < 0$. The total field is then

$$\vec{E}^I = \begin{cases} \vec{E}^i + \vec{E}^r\left(\vec{J}_1\right) & y > 0 \\ 0 & y \le 0 \end{cases} \tag{2}$$

Here, $\vec{J}_1$ is the surface current density on an infinite perfectly conducting half space when illuminated by a plane wave. According to the boundary condition for the tangential electric field on the ground plane, current density on the ground plane can be calculated easily by

$$\vec{J}_1 = 2\hat{y}\times\vec{H}^i = \frac{2}{\eta}\sin\varphi^i e^{jkx\cos\varphi^i}\hat{z}\,, \text{ on } S_1\,. \tag{3}$$

Here, η is the intrinsic impedance of free space and $\vec{H}^i$ is the magnetic field component of the incident plane wave on the ground plane.

In the presence of the discontinuity there will be three different kinds of field components, $\vec{E}^{p1}$, $\vec{E}^{p2}$, and $\vec{E}^S$. $\vec{E}^{p1}$ is the first type of perturbated field corresponding to the effect of discontinuity on the ground plane; $\vec{E}^{p2}$ is the second type of perturbated field due to the current density on the vanished region, as a result of the discontinuity ($x_1 < x < x_2$), shown in Figure 2; and $\vec{E}^S$ is the field scattered from the discontinuity. The total fields on surfaces S_1 and S_2 are

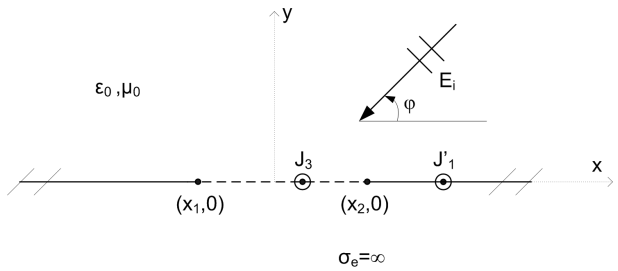

Figure 2. Demonstration of the vanished ground plane region.

$$\vec{E}^{i}+\vec{E}^{r}\left(\vec{J}_1\right)+\vec{E}^{p1}\left(\vec{J}_1^{p}\right)+\vec{E}^{S}\left(\vec{J}_2\right)+\vec{E}^{p2}\left(\vec{J}_3\right)=0\,. \tag{4}$$

Here, $\vec{J}_2$ is the electrical current density on the cylindrical discontinuity, $\vec{J}_1^{p}$ is the induced perturbated current density on S_1 due to the discontinuity, and $\vec{J}_3$ is the current density vanished due to the presence of the discontinuity, which is the negative of $\vec{J}_1$:

$$\vec{J}_3=-\vec{J}_1 \text{ on } S_3. \tag{5}$$

On S_1, $\vec{E}^{i}+\vec{E}^{r}$ is zero according to Eq. (2), so Eq. (4) becomes

$$\vec{E}^{p1}\left(\vec{J}_1^{p}\right)+\vec{E}^{S}\left(\vec{J}_2\right)=-\vec{E}^{p2}\left(\vec{J}_3\right). \tag{6}$$

At this point, formulations for bump and indent problems deviate. For the cavity problem, owing to Eq. (2), the scatterer cross-section will be in the region $y<0$ where there is not any incident or reflected fields when the cavity was absent. On the other hand, for the bump geometry, the scatterer cross-section will be in the region $y>0$ where incident and the reflected fields exist. Thus, for the bump problem, the fields on S_2 satisfy

$$\vec{E}^{p1}\left(\vec{J}_1^{p}\right)+\vec{E}^{S}\left(\vec{J}_2\right)=-\vec{E}^{i}-\vec{E}^{r}\left(\vec{J}_1\right)-\vec{E}^{p2}\left(\vec{J}_3\right) \tag{7}$$

and for the indent problem fields on S_2 satisfy

$$\vec{E}^{p1}\left(\vec{J}_1^{p}\right)+\vec{E}^{S}\left(\vec{J}_2\right)=-\vec{E}^{p2}\left(\vec{J}_3\right) \tag{8}$$

After applying point matching with pulse basis functions, for the bump problem, an equation set in matrix form is obtained as

$$\begin{bmatrix} Z_{nm} & Z_{lm} \\ Z_{nh} & Z_{lh} \end{bmatrix}\begin{bmatrix} J_n^{p} \\ J_l^{2} \end{bmatrix}=-\begin{bmatrix} E_m^{p2} \\ E_h^{i}+E_h^{r}+E_h^{p2} \end{bmatrix} \tag{9}$$

and in the case of an indent in the form of

$$\begin{bmatrix} Z_{nm} & Z_{lm} \\ Z_{nh} & Z_{lh} \end{bmatrix}\begin{bmatrix} J_n^{p} \\ J_l^{2} \end{bmatrix}=-\begin{bmatrix} E_m^{p2} \\ E_h^{p2} \end{bmatrix}. \tag{10}$$

Here, the impedance matrix elements are

$$Z_{io}=\frac{k\eta}{4}\int\limits_{C_i} H_0^{(2)}\left(k\left|\vec{r}_o-\left(\vec{r}_i+l'\,\hat{I}_i\right)\right|\right)dl'\,,i=n.l,\;\; o=m,h \tag{11}$$

where C_i indicates the ith source segment, $\vec{r}_i$ is the center of the source segment, $\hat{I}_i$ is the unit vector tangent to the source segment, $\vec{r}_o$ is the center of the oth observation segment, $l^{'}$ is the parametric integration variable defined on the corresponding source segment, and $H_0^{(2)}(\cdot)$ is the Hankel function of the second kind of order zero. Using Eq. (3), the perturbated field excited by vanished current $\vec{J}_3$ is

$$\begin{aligned} E_{m,h}^{p2} &= \frac{k\eta}{4}\int_{x_1}^{x_2} J_3\left(x^{'}\right) H_0^{(2)}\left[k\sqrt{\left(x_{m,h}-x^{'}\right)^2+y_{m,h}^2}\right] dx^{'} \\ &= \frac{k}{2}\sin\varphi^i \int_{x_1}^{x_2} e^{jkx^{'}\cos\varphi^i} H_0^{(2)}\left[k\sqrt{\left(x_{m,h}-x^{'}\right)^2+y_{m,h}^2}\right] dx^{'}, \end{aligned} \tag{12}$$

and

$$E_h^i+E_h^r = 2je^{jkx_h\cos\varphi^i}\sin\left(ky_h\sin\varphi^i\right). \tag{13}$$

J_n^p and J_l^2 currents can be calculated by solving the matrix equations of Eq. (9) or (10). Here, the energy is bounded on the intersection points x_1 and x_2. Calculation of the integrals on Eqs. (11) and (12) can be done numerically by adaptive Lobatto rule [24]. The scattered field is calculated after solving the currents by

$$E^S = E^{p1}\left(J^p\right)+E^S\left(J^2\right) \tag{14}$$

As a result, the scattered electric field can be calculated from

$$E^S = \frac{jk\eta}{4}\sqrt{\frac{2j}{\pi kr}}e^{-jkr}\left[\sum_{n=1}^{N_1} J_n^p\Delta_n e^{jk(x_n\cos\varphi^o+y_n\sin\varphi^o)}+\sum_{l=1}^{N_2} J_l^2\Delta_l e^{jk(x_l\cos\varphi^o+y_l\sin\varphi^o)}\right]. \tag{15}$$

Here, φ^o is the observation angle, and r is the distance measured from the origin to the observation point. Lastly, scattering width is defined as:

$$\sigma = \lim_{r\to\infty}\left[2\pi r\left|\frac{E^S}{E^i}\right|^2\right] \tag{16}$$

3. Numerical results

In order to show the validity of the method, the bistatic scattering width of a semicircular bump with $ka = 2\pi$ and normal incidence ($\varphi^i = 90^\circ$) in Figure 3a is compared with the series solution result [25]. In Figure 3b monostatic results ($\varphi^i, \varphi^o = 90^\circ$) are represented for varying ka. In these cases the perturbation current calculation domain length is chosen as $l = 5\lambda + 2a$, where a is the bump radius.

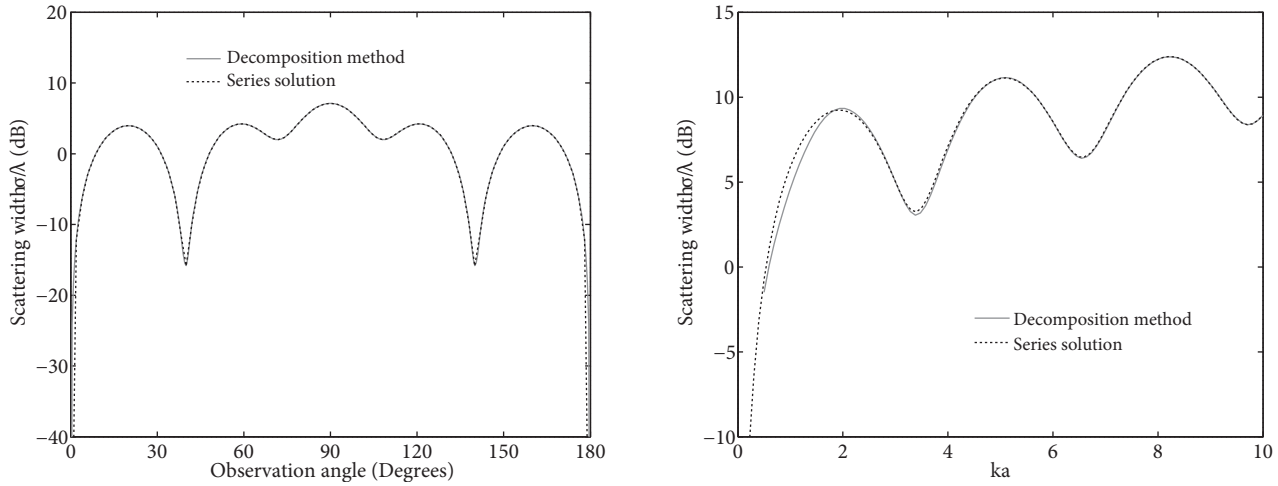

Figure 3. Scattering width of the circular bump normalized by wavelength: (a) with respect to observation angle, (b) ka.

As can be seen in Figure 3a, the results are in near excellent agreement, except for near grazing angles. Similarly, results versus ka are in very good agreement, except for low frequencies, where l is not wide enough for the perturbation current to decay, as is expected.

Afterwards the convergence of the solution with the change of the strip width l is investigated, and results are shown in Figure 4a as mean error ratio of current and error ratio for far-field results at observation angle ($\varphi^o = 90°$), compared to the reference MoM solution for $ka = \pi$ in the vicinity of normal ($\varphi^i = 90°$) plane wave incidence. Both results converge to the numerical error level while l/λ approaches 2.5. At this point it should be noted that proper selection of l is not only dependent on wavelength but also on bump size. Results presented in Figure 4a are calculated at 300 MHz and a semicircular bump with radius of 1 m. Mean error ratio for current density is calculated as:

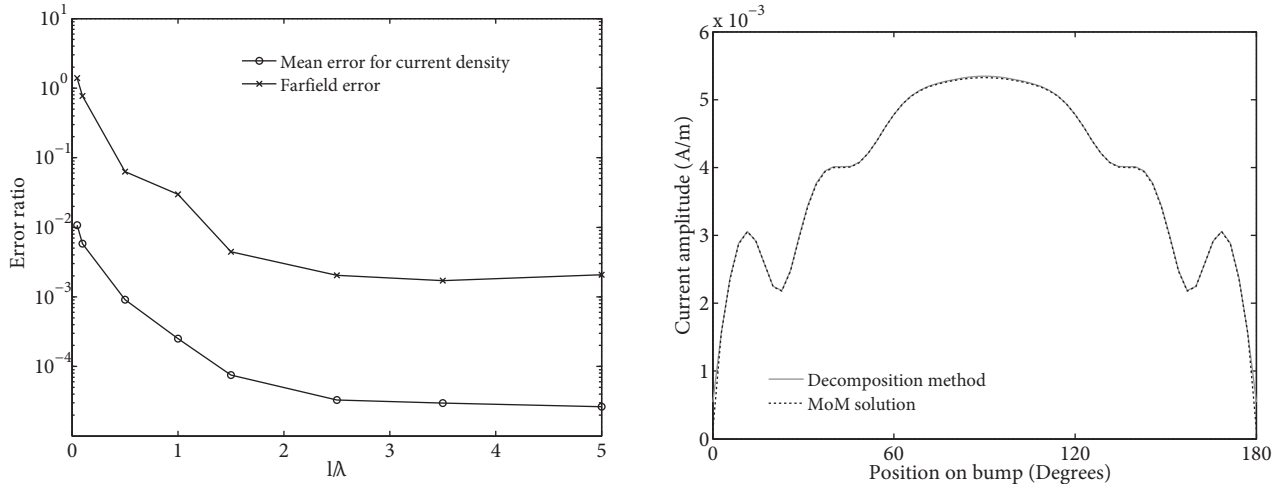

Figure 4. (a) Convergence of the solution with strip length, (b) current distribution comparison for $l/\lambda = 5$.

$$\text{Error} = E\left[\frac{|J^{dec} - J^{MoM}|}{|J^{MoM}|}\right] \tag{17}$$

and the far-field error is calculated as:

$$\text{Error} = \frac{\left|E^{dec} - E^{MoM}\right|}{\left|E^{MoM}\right|}. \tag{18}$$

Here, J^{dec} and J^{MoM} are current densities on the circular bump calculated by decomposition method and MoM, respectively; E^{dec} and E^{MoM} are scattered field calculated by two methods; and $E[\cdot]$ is the mean value operator.

Monostatic scattering width of a triangular bump, shown in Figure 5a versus observation angle, is presented in Figure 5b for the MoM solution. The bump has a base width of $8\ \lambda$ and a height of $2\ \lambda$.

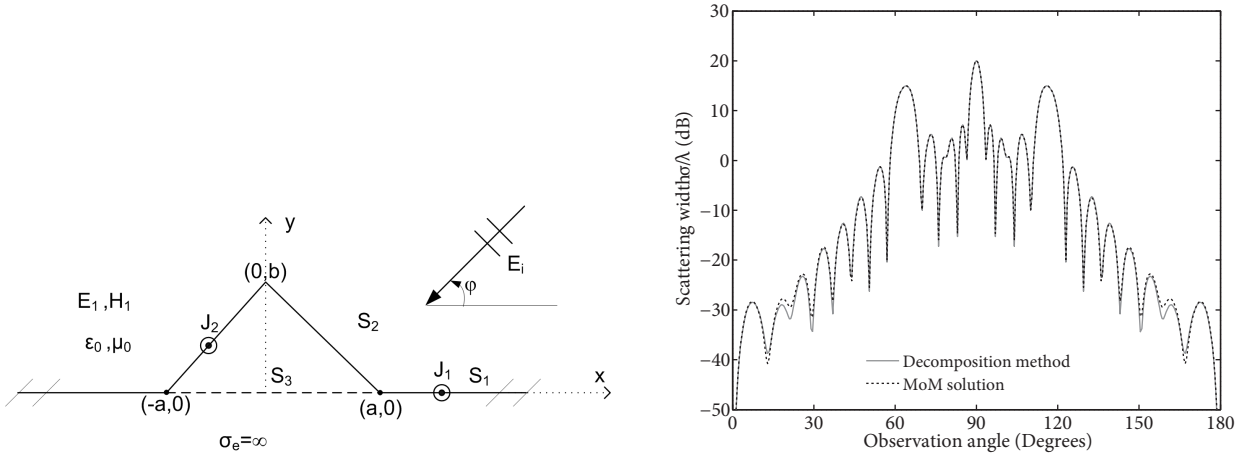

Figure 5. (a) Triangular bump geometry, (b) calculation results.

Results are almost identical except around 20° and 160°. Peaks around 60° and 120° correspond to reflections from the flat surfaces of the bump.

Backscattered scattering cross length for semicircular cavity in a perfectly conducting ground plane with $ka = 4\pi$ is shown in Figure 6 with the result from [4]. Reference and calculated results are nearly indistinguishable, and it is thought that errors made during data extraction from the reference article may have caused the small deviations seen.

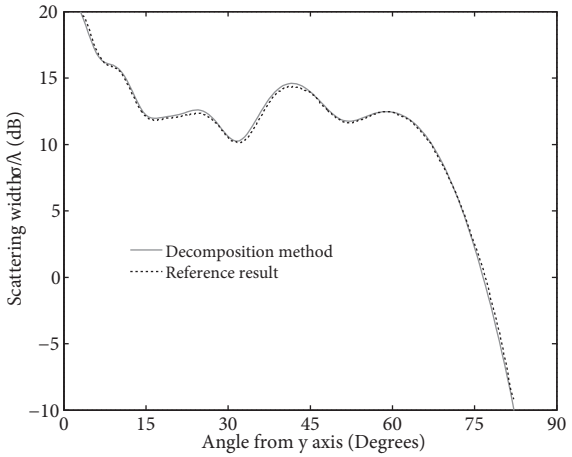

Figure 6. Calculation result for semicircular cavity.

Next, the semielliptical cavity in a ground plane geometry depicted in Figure 7a is investigated for different eccentricity values. The backscattered normalized field versus ka is compared with results of [5] in Figure 7b. Again the results agree very well, except for minor offset error along the ka axis, which is due to data extraction artifacts and low frequency deviations explained for the case in Figure 3b.

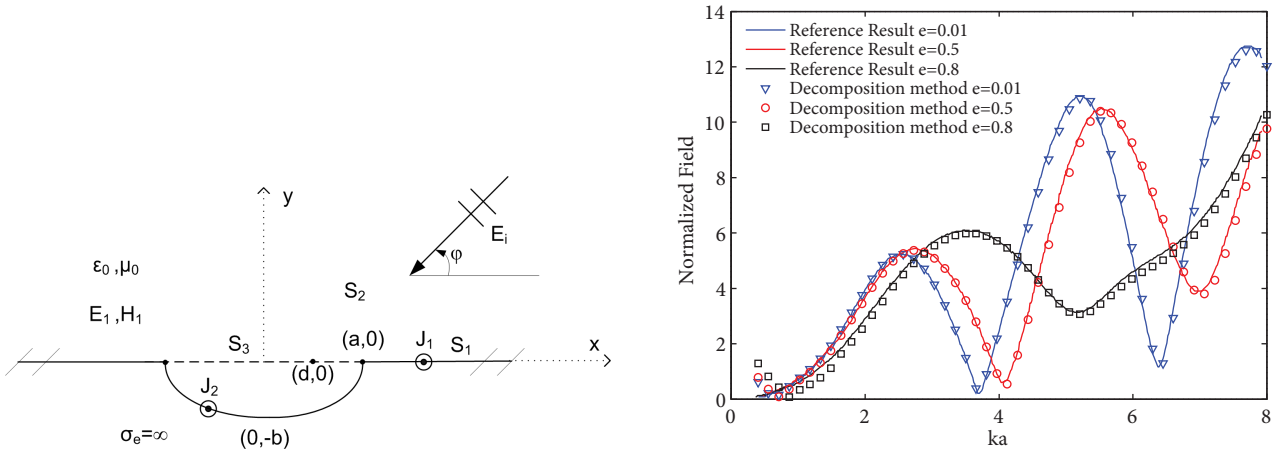

Figure 7. (a) Semielliptical cavity geometry, (b) calculation results.

Lastly, rectangular and triangular cavity geometries shown in Figure 8a are examined and simulation results are compared with reference publications [14] and [15] in Figure 8b. For the rectangular geometry, a and b values are $0.6\ \lambda$ and $0.8\ \lambda$, respectively, and for the triangular geometry a and b are $0.75\ \lambda$ and $1.65\ \lambda$.

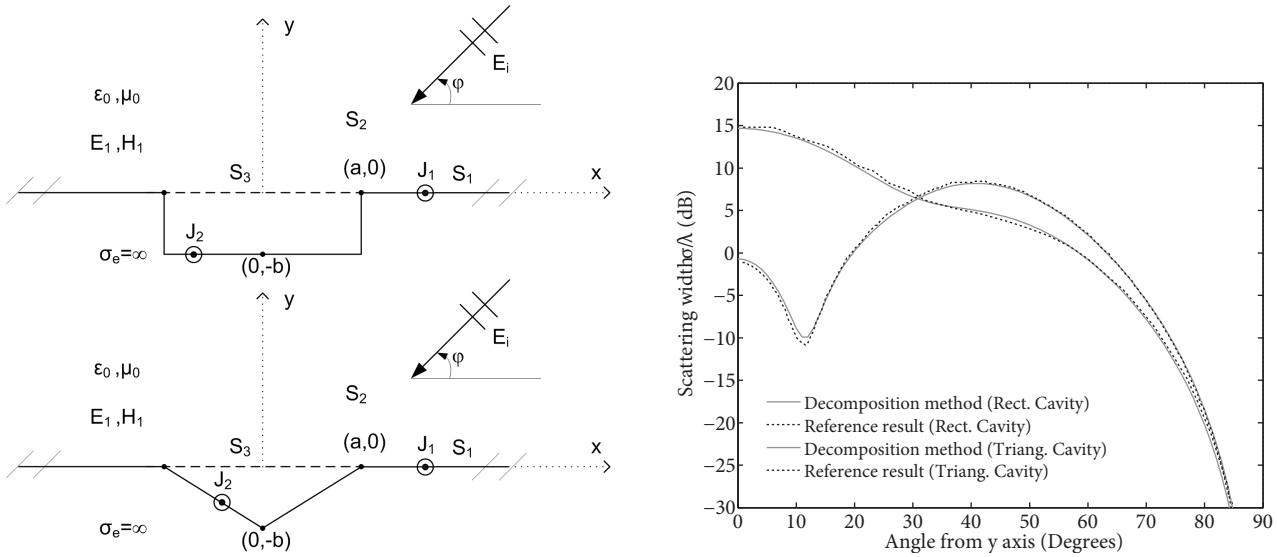

Figure 8. (a) Rectangular and triangular cavities, (b) calculation results.

4. Conclusion

A new numerical solution method for solving electromagnetic scattering from discontinuities on an infinite perfectly conducting ground plane is presented for TM polarization. Calculation results for various validation

cases show very good agreement with proper choice of truncation widths. The solution procedure is simple, based on the solution of a single type of integral equation, and can be generalized to various other problems. In the future both lossy structures and ground planes with roughness will be examined.

References

[1] Twersky V. On scattering and reflection of electromagnetic waves by rough surfaces. IRE T Anten Propag 1957; 5: 81-90.

[2] Hansen T, Yaghjian A. Low frequency scattering from two dimensional perfect conductors. IEEE T Anten Propag 1992; 40: 1389-1402.

[3] Hansen T. Uniqueness theorems for static integral equations and calculations of constants for 2-D low frequency scattering. IEEE T Anten Propag 1993; 41: 1916-1921.

[4] Hinders MK, Yaghjian AD. Dual series solution to scattering from a semicircular channel in a ground plane. IEEE Microw Guided W 1991; 1: 239-242.

[5] Byun W, Yu J, Myung N. TM scattering from hollow and dielectric filled semielliptic channels with arbitrary eccentricity in a perfectly conducting plane. IEEE Trans Microw Theory 1998; 46: 1336-1339.

[6] Tyzhnenko A. Two-dimensional TE-plane wave scattering by a dielectric-loaded semicircular trough in a ground plane. Electromagnetics 2004; 24: 357-368.

[7] Senior TBA, Volakis JL. Scattering by gaps and cracks. IEEE T Anten Propag 1989; 37: 744-750.

[8] Buyukaksoy A, Birbir A, Erdogan E. Scattering characteristics of a rectangular groove in a reactive surface. IEEE T Anten Propag 1995; 43: 1450-1458.

[9] Barkeshli K, Volakis JL. Scattering from narrow rectangular filled grooves. IEEE T Anten Propag 1991; 39: 804-810.

[10] Senior TBA, Sarabandi K, Natzke JR. Scattering by a narrow gap. IEEE T Anten Propag 1990; 38: 1102-1110.

[11] Wood WD, Wood W. Development and numerical solution of integral equations for electromagnetic scattering from a trough in a ground plane. IEEE T Anten Propag 1999; 47: 1318-1322.

[12] Wood WD. Electromagnetic scattering from a cavity in a ground plane: theory and experiment. PhD, Air Force Institute of Technology, Dayton, OH, USA, 1997.

[13] Jin J, Volakis J. A finite element boundary integral formulation for scattering by three dimensional cavity backed apertures. IEEE T Anten Propag 1991; 39: 97-104.

[14] Jin J. Electromagnetic scattering from large, deep, and arbitrarily shaped open cavities. Electromagnetics 1998; 5: 3-34.

[15] Chumachenko VP, Karucuha E, Dumanli M. TM scattering from a multiangular groove in a ground plane. J Electromagn Waves Appl 2000; 14: 329-347.

[16] Huang J, Wood A. Numerical simulation of electromagnetic scattering induced by an overfilled cavity in the ground plane. IEEE Antenn Wireless Propag Lett 2005; 4: 224-228.

[17] Xu Y, Wang C, Gan Y. Two integral equations for modeling electromagnetic scattering from indented screens. IEEE T Anten Propag 2005; 53: 275-282.

[18] Wood A. Analysis of electromagnetic scattering from an overfilled cavity in the ground plane. J Comput Phys 2006; 215: 630-641.

[19] Kızılay A. A perturbation method for transient multipath analysis of electromagnetic scattering from targets above periodic surfaces. PhD, Michigan State University, East Lansing, MI, USA, 2000.

[20] Kizilay A., Rothwell EJ. Perturbation method solution of TE scattering from a cylinder above an infinite periodic surface. In: Antennas and Propagation Society International Symposium; 21–26 June 1998; Atlanta, GA, USA. New York, NY, USA: IEEE. pp. 1304-1307.

[21] Makal S, Kizilay A. Computation of the scattered fields from a dielectric object buried in a medium with a periodic surface by a decomposition method. IET Microw Antenna P 2011; 5: 1703-1709.

[22] Xu XB, Butler C. Scattering of TM excitation by coupled and partially buried cylinders at the interface between two media. IEEE T Anten Propag 1987; 35: 529-538.

[23] Asvestas J, Kleinman R. Electromagnetic scattering by indented screens. IEEE T Anten Propag 1994; 42: 22-30.

[24] Gander W, Gautschi W. Adaptive quadrature—revisited. BIT 2000; 40: 84-101.

[25] Bowman JJ, Senior TBA, Uslenghi PLE. Electromagnetic and Acoustic Scattering by Simple Shapes. Amsterdam, the Netherlands: North Holland, 1969. pp 103-108.